

**LL-CHONDRITE NORTHWEST AFRICA 6813: SAMPLING AN IMPACT-CRATERED ASTEROID.**

L. Hoare<sup>1</sup>, M. Schmieder<sup>2,3</sup> and D. A. Kring<sup>2,3</sup>, <sup>1</sup>School of Earth Sciences, University of Bristol, Wills Memorial Building, Queens Road, Bristol, BS8 1RJ, UK ([lh13670@my.bristol.ac.uk](mailto:lh13670@my.bristol.ac.uk)) <sup>2</sup>Lunar and Planetary Institute, 3600 Bay Area Boulevard, Houston, TX 77058, <sup>3</sup>NASA Solar System Exploration Research Virtual Institute.

**Introduction:** Impact cratering is one of the dominant geologic processes affecting asteroids. It results in shock-induced melting and the formation of impactites, including impact melt breccias. Meteoritic samples of these breccias possess petrologic and geochemical signatures that can be used to deduce the collisional evolution of the respective parent body, such as the timing of the event, shock metamorphic conditions during the impact, subsequent two-stage cooling, and an estimate of the size of the impact crater itself. In this study we analyzed the petrography and mineral chemistry of Northwest Africa (NWA) 6813 in order to elucidate its thermal and impact history. NWA 6813 was classified as an LL6 impact melt breccia [1], which is part of a group of ordinary chondrites whose impact lithologies remain poorly described.

**Analytical Methods:** We examined a thin-section (DKLPI-174) of NWA 6813. To determine modal abundances, a point count (n=4296) was conducted on a petrographic microscope at  $\times 500$  magnification, with a step size of 100  $\mu\text{m}$  along lines with a separation of 300  $\mu\text{m}$ . To determine chemical compositions, analyses were made with a JEOL 8530F electron microprobe at the NASA-JSC using an accelerating voltage 15 kV. Silicates were analysed using a 20 nA beam current and a 1  $\mu\text{m}$  beam diameter. Feldspar was analysed using a 10 nA beam current and a 2-4  $\mu\text{m}$  beam diameter. Metal and sulphide were analysed using a 30 nA beam current and a 1  $\mu\text{m}$  beam diameter (metal) and 3  $\mu\text{m}$  (sulphide). Some metal analyses were conducted along line scans with an analytical spacing of 2-4  $\mu\text{m}$ .

**Petrography:** The sample is an impact-brecciated LL-chondrite with melt veins and pockets, and is composed of two distinct lithotype domains: (i) a clast domain (CD), which is composed of 5 distinctive clasts, with two large clasts (1 and 5) 6.3 $\times$ 7.7 mm and 6.7 $\times$ 8.5 mm, and (ii) an optically dark, melt-bearing (DMB) domain that surrounds small entrained clast fragments and contains veins and pockets of impact melt (Fig. 1). The CD is  $\sim 68\%$  of the sample. Clast 5 appears darker than the other clasts.

**Clast domain.** This domain is composed of 84% silicates, oxides, 3% metals, 4% sulphides, and 7% undivided metal/sulphides ( $< 4 \mu\text{m}$  in size), normalised to 100%, which is consistent with the modal composition of other LL-chondrites [2]. Chondrules have mostly porphyritic olivine, barred olivine, and radial pyroxene textures, and fewer porphyritic olivine-pyroxene textures. The average

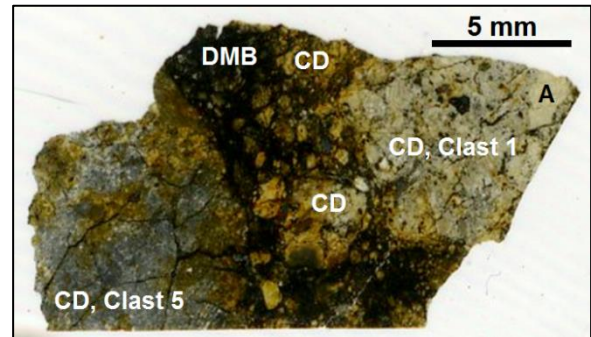


**Figure 1.** Thin section scan showing the clast domain (CD) and the dark, melt-bearing (DMB) domain.

chondrule diameter is  $\sim 570 \mu\text{m}$ , which is comparable to that in other LL-chondrites [3]. Hypidiomorphic olivine crystals are locally up to  $\sim 300 \mu\text{m}$  in size. Pyroxene and rare interstitial feldspar grains are up to  $\leq 200 \mu\text{m}$  in size. Mono- and poly-mineralic metal, sulphide, and oxide grains are up to 400  $\mu\text{m}$  in size. Clast 1 contains a large (2.1 $\times$ 2.9 mm) olivine-pyroxene object (A in Fig. 1), with an orthopyroxene oikocryt poikilolitically enclosing smaller euhedral olivine grains.

**Dark, melt-bearing domain.** This domain is 84% silicates, 4% oxides, 2% metals, 1% sulphides, and 9% undivided metal/sulphide ( $< 4 \mu\text{m}$  in size), normalised to 100%. Clast fragments are rounded to irregular in shape, light coloured, and suspended in an optically dark 'matrix' (Fig. 1). Individual relic subhedral olivine and pyroxene crystals are present within the optically dark regions and are typically  $\sim 15$  to  $\sim 300 \mu\text{m}$  in size. Localised pockets or veins of impact melt contain orbicular metal-sulphide particles and partially melted clast fragments, both typically  $\sim 5$ – $30 \mu\text{m}$ , within a cryptocrystalline melt matrix (Fig. 2).

**Geochemistry:** Olivine is  $\text{Fa}_{25.2-30.4}$  (n=56), dominated by  $\text{Fa}_{28-29}$ , which is consistent with compositions in other LL-chondrites [4]. Some pyroxene crystals are zoned, with low-Ca cores and high-Ca rims of pigeonite, and rarely augite. High-Ca pyroxene ( $> 5\%$  Wo) is  $\text{Wo}_{5-43}\text{En}_{47-75}\text{Fs}_{10-21}$  (n=6). Low-Ca pyroxene is  $\text{Wo}_{0-1.4}\text{En}_{69-89}\text{Fs}_{11-30}$  (n=65). Values of FeO/MnO for olivine, low-Ca pyroxene, and high-Ca pyroxene are 57.2–58.0, 33.9–36.7, and 30.2–32.2, respectively, all of which are comparable to ratios of other LL-chondrites [5,6]. Feldspar is  $\text{Ab}_{29.5-88.4}\text{Or}_{1.7-71.8}\text{An}_{1.7-28.1}$  (n=77) and most are highly sodic ( $\text{Ab} > 75$ ). Nickel concentrations in taenite range from 23.9 to 38.6 wt%. Kamacite contains an average of 2.8

wt% Co, which falls within the typical range for LL-chondrites [7]. Sulphide is dominantly troilite. Pyroxene in the olivine-pyroxene object of clast 1 (A, Fig. 1) exhibits a distinctive trend with  $\text{TiO}_2$  and  $\text{Al}_2\text{O}_3$  increasing as CaO increases.

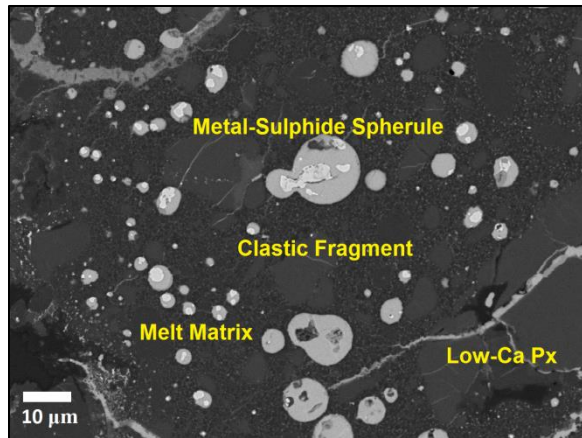


**Figure 2.** BSE image of an impact melt pocket in the dark, melt-bearing domain, with metal-sulphide droplets and entrained relict mineral clasts (mostly olivine) in a cryptocrystalline melt matrix. Cross-cutting shock veins and fractures are also present.

**Metamorphism:** *Thermal Metamorphism.* Olivine in the clasts is relatively homogeneous, whereas pyroxene compositions are more variable. Low-Ca pyroxene is predominantly orthorhombic, chondrule rim sharpness is well-defined to readily delineated, and feldspar occurs predominantly in microcrystalline aggregates  $\leq 50 \mu\text{m}$ , all of which indicates a thermal metamorphic type 4–5 for the chondrite [4]. Some chondrules contain turbid igneous glass, and the matrix is a mixture of transparent microcrystalline and recrystallised material, indicative of type 4–5 [4]. The maximum Ni content of kamacite and taenite, is  $>20 \text{ wt}\%$ , and the average Ni content of sulphide minerals is  $<0.5 \text{ wt}\%$ , which suggests type 4 and above [4]. In clast 5, chondrules are typically poorly defined, and feldspar interstitial grains are  $\geq 50 \mu\text{m}$ , with some up to  $300 \mu\text{m}$  in size, within a predominantly recrystallized matrix, suggesting type 5–6 [4]. The grade of thermal metamorphism is not uniform across the sample, which is dominantly composed of LL5 clasts with a subordinate LL6 component (clast 5).

*Shock Metamorphism.* Undulatory extinction, planar fractures, and mosaicism were present in 20 randomly selected olivine crystals in the clasts indicating a shock stage S5–6, although the sample lacks apparent ringwoodite and significant maskelynite. The presence of ubiquitous veins and pockets of impact melt (Fig. 2), suggest a shock stage of S6; i.e., shock pressures of  $\sim 45\text{--}90 \text{ GPa}$  and a post-shock temperature increase of  $600\text{--}1750^\circ\text{C}$  [8],

consistent with the initial classification as an impact melt breccia [1], although our sample does not clearly display a melt matrix.

**Metallography:** Metal textures range from distinctly zoned particles of kamacite and taenite to rare plessite. Small metal-sulphide spheres are present in the impact melt and some contain small ( $\sim 2\text{--}5 \mu\text{m}$ ) metal cells. A tentative stage 1 cooling rate for the superheated melt was calculated using the method of Scott [9]. Cell widths of  $2\text{--}5 \mu\text{m}$  suggest a tentative stage 1 cooling rate of  $\sim 5000\text{--}70000^\circ\text{C}/\text{sec}$ . No meaningful stage 2 cooling rate could be calculated due to the high Ni content ( $>20\text{--}50 \text{ wt}\%$ ) of the metal [10], characteristic of LL-chondrites [11]. However, cooling was presumably (very) fast. High Ni in troilite ( $>0.1 \text{ wt}\%$ ) and the small size of metal-sulphide melt orbs also indicate fast cooling.

**Discussion:** The heterogeneity in petrologic type is possibly the result of impact brecciation and mixing at depth in a large crater. Alternatively, a smaller impact event may have melted a near-surface breccia produced previously by older impact events. The distinct trends in  $\text{TiO}_2$  and  $\text{Al}_2\text{O}_3$  in the unusual olivine-pyroxene object in clast 1 could be the result of igneous processes and, thus, the object could be an achondritic fragment, potentially of LL-derivation, based on Fa# and FeO/MnO values of olivine. If produced on the same parent body, that clast might require excavation from greater depth than type 6 material in either of the rock-forming scenario.

**Conclusions:** Our sample represents an LL5 melt-bearing impact breccia, probably formed within the structural floor of an impact crater. The NWA 6813 parent asteroid experienced thermal metamorphism to an LL5/6 stage, followed by S6 shock metamorphism. The heterogeneity in petrologic type could be the result of impact-related brecciation and/or impact-melting and mixing of various lithologies in the asteroid target. Prior to the impact event, LL5/6 material and some igneous material had possibly been present at, or near the asteroid surface. After the impact, the melt-bearing impact breccia underwent rapid two-stage cooling.

**References:** [1] Rubin A. E. (2012) *The Meteoritical Bulletin*, #99. *MAPS*, 47(11), 38. [2] Weisberg M. K. et al., (2006) in *Meteorites and the Early Solar System II*, 19-52. [3] Rubin A. E. (2000) *Earth Sci. Rev.* 50, 3-72. [4] Van Schmus W. R. and Wood J. A. (1967) *GCA*, 31, 747-76. [5] Rubin A. E. and Swindle T. D. (2011) *MAPS*. 46, 587-600. [6] Rubin A. E. (2000) *GCA*, 66, 3327-3337. [7] Afiattalab F. and Wasson J. T. (1980) *GCA*, 44, 431-446. [8] Stöffler D. et al., (1991) *GCA*, 55, 3845-3867. [9] Scott E. R. D. (1982) *GCA*, 46, 813-832. [10] Jarosewich E. (1990) *Meteoritics*, 25, 323-337. [11] Willis. J and Goldstein J. I. (1981) *Proc. Lunar Planet. Sci.*, 12B, 1135-1143.